

# Solar Battery Chargers for NiMH Batteries

Florent Boico, Brad Lehman, *Member, IEEE*, and Khalil Shujaee

**Abstract**—This paper proposes new solar battery chargers for NiMH batteries. First, it is shown that existing charge-control methods can fail when charging by solar arrays in changing environmental conditions. This article discusses the reasons for the failure and introduces new voltage and temperature-based charge-control techniques. To increase charge speed, a maximum power point tracker is also implemented within the micro-controller of the proposed charger.

**Index Terms**—Battery charger, maximum power point, solar.

## I. INTRODUCTION/PROBLEM MOTIVATION

RECENT technological developments in thin-film photovoltaics (PVs), such as amorphous silicon [1], [2] and hybrid dye sensitized/PV cells [3], are leading to new generations of consumer portable solar arrays. These new arrays are lightweight, durable, flexible, and have been reported to achieve power efficiencies of up to 10% [1]. Already, commercial-off-the-shelf arrays exist that have panels embedded in fabric that can be folded to dimensions of less than 12" × 12", yet are able to produce up to 50 W of power [1] at 12 V. These new products make solar power available to hikers, campers, soldiers-on-the-move, etc., since the arrays can now be easily carried in backpacks. Thus, the marketplace for portable solar power is beginning to broaden beyond its conventional (original) boating and recreational vehicle (RV) market.

Older solar battery chargers (for RVs and boats) were primarily developed to recharge gel cell and lead acid batteries [4]. However, since the emergence of these flexible and foldable solar arrays, there has become a need to develop solar battery chargers for more portable batteries, such as NiMH and/or Li-ion batteries that can be carried by hikers. However, charging these types of batteries with solar power leads to new research challenges that have yet to be discussed in the literature, such as: Is it possible to fast charge batteries with solar arrays in unknown outdoor environmental conditions? How should ambient temperature swings, changing illumination conditions, and other environmental changes be incorporated into charge-control algorithms? Should maximum power point tracking (MPPT) be used? What are the best battery charger system architectures for these portable solar arrays? etc.

The purpose of this paper is to answer these and other open research challenges for NiMH batteries being charged by the

portable solar arrays. Although we present the results for NiMH batteries, they can also be applied to NiCd batteries, as we explain below. We present the following contributions.

- First, in Section II of this paper, we show that existing, conventional [5]–[9] charge-control algorithms cannot be used to properly charge NiMH batteries when used with these portable (mid-power) solar arrays. Specifically, changing weather conditions, such as light illumination, temperature, wind, etc., can actually “trick” conventional charge controllers to believing that the battery is fully charged. Hence, charging would be falsely terminated when existing battery charging IC’s [9] are used.
- Section III presents new, robust and reliable charge-control algorithms that are suitable for charging NiMH batteries with portable solar arrays. These algorithms can easily be adapted into existing battery charger ICs [9]. One algorithm relies on the battery voltage while a second algorithm relies on the derivative of temperature. Unique to both algorithms is that they include specialized reset mechanisms to eliminate false charge termination due to changing illumination conditions, ambient temperature swings or other environmental changes. Either of these two algorithms can be used separately, but they may also be combined to improve the system robustness.
- Section IV gives background on different MPPT techniques and then proposes a MPPT system architecture for the charger that includes a bypass switch. The new charger with MPPT leads to faster charging of wider ranges of battery terminal voltages.

A prototype charger has been designed, built and experimentally tested. Field experiments verify that the charger is: 1) robust and reliable for solar battery charging NiMH batteries; 2) compact; and 3) that the addition of MPPT [10], [11] with a bypass switch inside the charger could maximize output power capabilities of the solar array while charging batteries with wider range of terminal voltages, e.g., 24 V, 12 V, 9 V, etc.

## II. OPEN CHALLENGES AND RESEARCH NEEDS

Different algorithms exist to detect when the battery reaches full state of charge (SOC). They can be classified into two different categories:

- Algorithms relying on records of the battery history and characteristics [12], [13].
- Algorithms requiring no prior knowledge of the battery characteristics, such as the  $dV/dt$  or temperature-based algorithms [5]–[8].

The first type of algorithms are suitable when the charge controller is monitoring the same battery all the time or when the battery is “smart,” that is, when a circuit recording capacity, state of charge and other internal characteristics are embedded inside the battery pack and capable of exchanging data with the charge-control circuit.

Manuscript received February 21, 2006; revised May 26, 2006. This work was supported by a grant from the Collaborative Technology Alliance/Army Research Laboratory. Recommended for publication by Associate Editor K. Ngo.

F. Boico and B. Lehman are with Northeastern University, Boston, MA 02115 USA (e-mail: boico.f@neu.edu; lehman@ece.neu.edu).

K. Shujaee is with Clark Atlanta University, Atlanta, GA 30314 USA (e-mail: kshujaee@cau.edu).

Color versions of one or more of the figures in this paper are available online at <http://ieeexplore.ieee.org>.

Digital Object Identifier 10.1109/TPEL.2007.904164

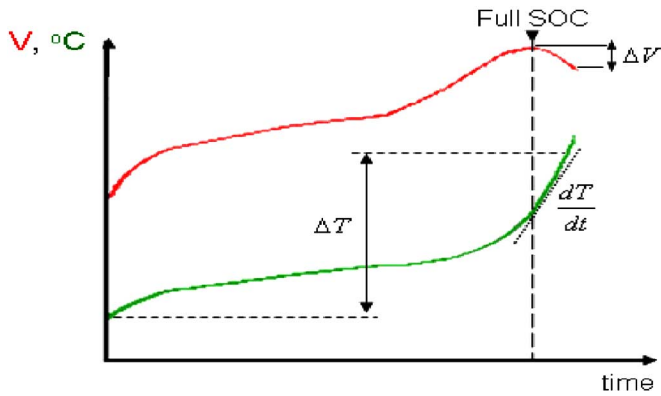


Fig. 1. NiMH voltage and temperature profile for constant current charging shows multiple methods available for detecting full SOC.

We focus our research on the second type of algorithm, as there is a need for a charger capable of charging a different battery each time. In addition, the overwhelming majority of general purpose batteries available are not of the smart type.

NiMH batteries are normally fast-charged by regulating the input power source to behave like a constant current source. Then, the constant charging current is applied to the battery until it is desired to terminate charging. Often, a trickle or top-off charge is added after the fast-charge in order to balance the charge between the battery cells. Fig. 1 illustrates how “fast-charge” termination time is typically determined, which we explain below.

#### A. Existing Voltage Detection Methods Fail When Charging NiMH Batteries with Portable Solar Arrays

Common approaches to determining when NiMH batteries (charged by constant current source) are fully charged rely on measuring battery terminal voltage [5]. Occasionally, the charge process is terminated when the battery’s voltage reaches a certain value. However, this is extremely unreliable and does not work when the battery is charged by different current levels or when it is placed in different ambient temperatures. Hence, it is not suitable for discussion here.

A second approach, which is more prevalent, is to stop the fast-charging process (a bit after the full SOC point) when battery terminal voltage begins to drop, i.e.,  $dV/dt < -K$ , where  $K$  is a positive fixed threshold value set by the user. This is commonly implemented by specifying a  $\Delta V$  drop in voltage as a threshold instead of calculating a derivative directly (around 10 to 20 mV per cell [5]). This is illustrated on the voltage plot in Fig. 1. However, once again, implicit in this approach is that the charging current remains constant during the charging process. This charging method is also valid for NiCd batteries, but typically with a higher threshold voltage drop.

We remark that there are other charging algorithms that have been published: In [6] and [8], overcharge is avoided by estimating the time derivative of the voltage. This approach although more accurate is also subject to the same limitations as conventional algorithms when facing changing illumination conditions. Another technique to detect full state of charge relies on the battery impedance changes with charging. However, in the case of NiMH chemistry, those changes are very small and require some precise model of the battery characteristics (usually involving battery history) [15].

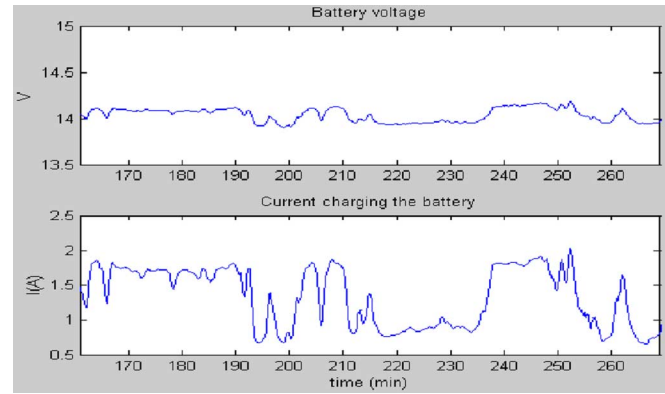


Fig. 2. Voltage of the NiMH battery charged with a solar array. Drops in the voltage, due to drops in the solar array current, are falsely detected as overcharge by classical charging algorithms.

#### B. Temperature Detection Issues

As Fig. 1 illustrates, when the battery approaches full SOC, temperature begins to rise sharply. This is true for either NiMH or NiCd batteries. Thus, another approach to determine full SOC is to place a thermistor close to battery cells. This enables detection of charge termination when  $dT/dt$  is above a threshold value.

Two temperature-detection methods are mainly used:

- When the change in battery temperature over the entire charge process (defined as  $\Delta T$ ) reaches a certain threshold, charge is stopped. This method is not very accurate for our outdoor application, since it works only if the ambient temperature is kept constant throughout the charging process.
- Charge is halted when the slope of the temperature curve rises above a threshold value.

Temperature-based detection is considered more accurate than voltage-based detection because the detection usually happens at full SOC. As Fig. 1 shows, voltage methods need to let the cell overcharge for a certain time until the voltage drop is detected.

Unfortunately, as with voltage-based detection, some challenges exist [7] when the battery is exposed to changing weather conditions.

- The change of temperature in the battery at overcharge ( $\Delta T$ ) differs depending on ambient temperature. Since the temperature can change greatly throughout the day, comparing current battery temperature to its value at the beginning of the charging process loses meaning.
- Ambient temperature swings can occur during the day due to the sunlight, and change in air and ground temperature. These changes can cause fast increases and decreases in battery temperature and also fool time-derivative-based algorithms.
- The rise in temperature due to overcharging is dependent on the average charging currents. Therefore, the threshold on  $dT/dt$  required for accurate detection changes with the average charging current (see Fig. 3).

Fig. 2 presents outdoor experimental data that helps explain why negative  $dV/dt$  (or  $-\Delta V$ ) detection cannot be directly used to determine end-of-charge time when the power source is a solar

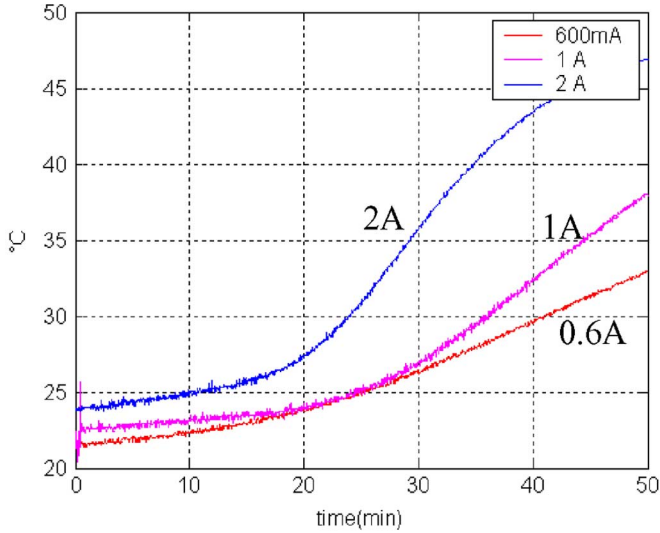


Fig. 3. Temperature elevation in the battery with different charging current (2 A, 1 A, and 600 mA). The threshold required on derivative of temperature for accurate full SOC detection varies greatly with the average current.

array. In Fig. 2, a 30-W portable solar array [1] is directly connected to a 12-V, 6 A-Hr NiMH battery, BB-390 [14] currently used by the U.S. Army. Notice that when clouds pass across the sun, the solar array's charging current decreases. This lowers the battery terminal voltage, due to the battery's internal resistance/impedance. Due to the battery's internal capacitance, the voltage continues to drop slowly until the charging process balances and the voltage starts to rise again. These drops are not negligible and are usually higher than the voltage drops due to overcharge. Moreover, they arise from weather changes and are, therefore, unpredictable. So, a charger using conventional voltage detection algorithms will falsely detect overcharge and stop the charge too early.

In summary, since existing charge-control algorithms and ICs are developed for constant ambient room temperature and constant preset charging current, they are not reliable and often fail when ambient temperatures vary, as in the case here.

### III. NEW CHARGE CONTROLLER ALGORITHMS

#### A. New Voltage-Based Algorithm

As we have seen, in Section II, a challenge with voltage-based full SOC detection is that it gets easily fooled by changing current. A primary cause of the change in charging current is due to clouds or shade on the solar panel. These changes create large voltage drops accompanied by a slow voltage decrease in the battery terminal voltage. The two effects combined are difficult to predict. However, they can be detected by sensing either a sudden drop in current or battery voltage. These events can be labeled as false alarms, and they can be incorporated into more sophisticated charge-control algorithms that do not prematurely stop charging the battery when these sudden changes occur.

A new proposed voltage detection algorithm is presented in Fig. 4. The algorithm does not get fooled by changing weather conditions. The idea is to keep track of the charging current and reset the algorithm whenever the current departs from an acceptable limit. This ensures that any voltage drop due to a

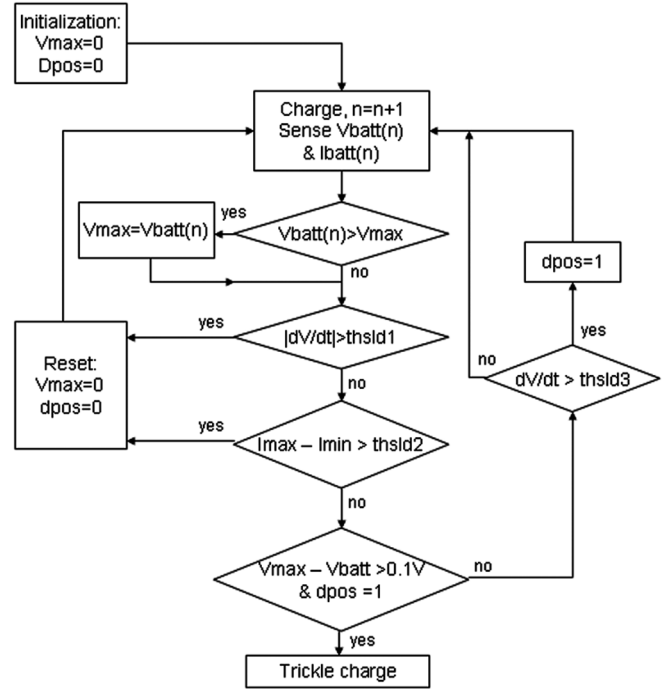


Fig. 4. New  $dV/dt$  algorithm proposed to overcome the false detection issue. Large drops of voltage or current reset the algorithm.

change in the current does not falsely trigger the end of charge. This leads to the condition that if the maximum or minimum of the charging current ( $I_{max}$ ,  $I_{min}$  on Fig. 4, recorded over a sliding window of around 5 min) departs from the average value above or below a certain threshold level, the algorithm should reset. Overcharge can only be detected after the current returns to a constant value (over a period of time) again.

Description of The New Voltage Control Algorithm: Referring to Fig. 4, at each time instant:

- the algorithm keeps track of the maximum battery voltage recorded by checking whether  $V_{batt}(n) > V_{max}$ ; if the voltage changes suddenly ( $|(dV)/(dt)| > thsl d1$ ) or if the current has recently varied by a substantial amount ( $I_{max} - I_{min} > thsl d2$ ), then the voltage measurement is not reliable anymore. The maximum is reset to prevent false detection of peaks at lower charging current (and therefore lower voltage peaks);
- to detect full SOC from the drop in the voltage (classical method) the algorithm requires, also, that the derivative of the voltage first rises significantly. This is detected when  $(dV)/(dt) > thsl d3$ . “ $dpos = 1$ ” means that a positive  $dV/dt$  has been detected. When  $dpos = 1$  and the voltage drops to a threshold below its maximum, the algorithm stops fast-charging.  $I_{max}$  and  $I_{min}$  are the max and min current of a 5- to 10-min sliding window.

It should be noted that because of the battery's internal capacitance, the battery voltage will continue to drop long after the current has stabilized. To avoid false detection (of full SOC) due to this phenomenon, the algorithm requires a positive  $dV/dt$  to rearm itself after it has reset. Therefore, the end of charge is based on both  $\Delta V$  and on the shape of the overall voltage curve when approaching overcharge.

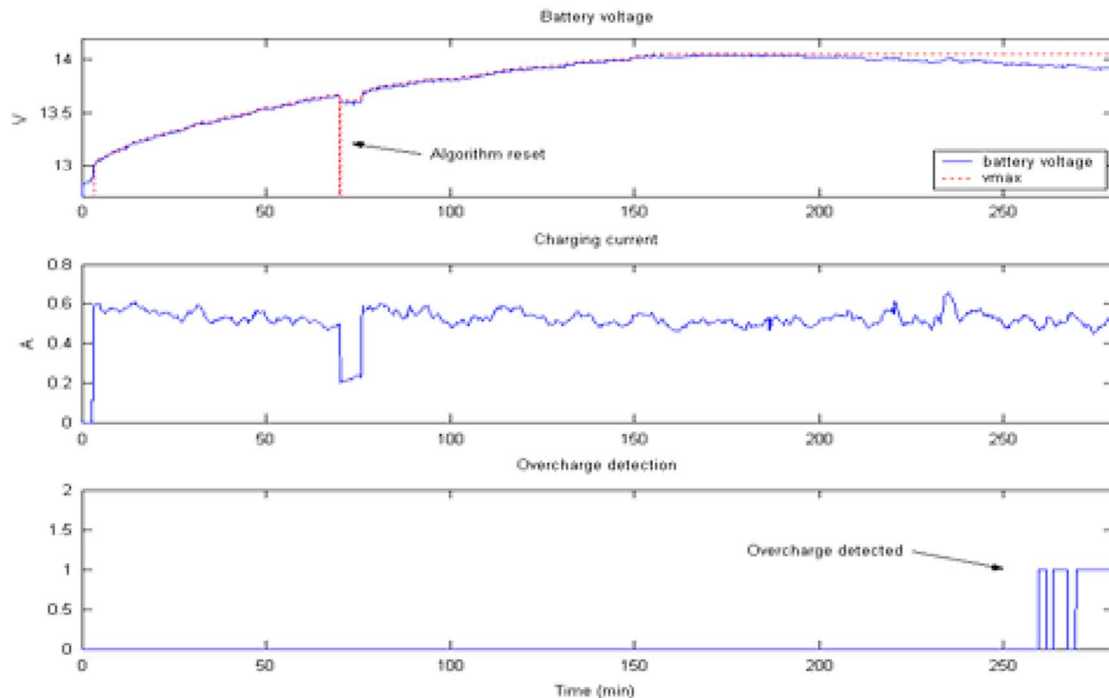


Fig. 5. Outdoor solar battery charging with new voltage detection charge-control algorithm. The algorithm has the ability to handle disturbances in the current. At  $t = 65$  min, the drop in the current (due to shade) is detected and the algorithm does not get fooled. At  $t = 260$  min, overcharge is detected. Conventional voltage detection algorithms falsely stop charging at  $t = 65$  min.

When charging with constant current, this algorithm performs the same as the conventional algorithm with (maybe) a higher requirement in the  $\Delta V$  threshold required to halt charging for robustness purpose ( $\Delta V_{\text{thslid}} = 0.1$  V for a 12-V NiMH battery or 10 mV per cell [5]). This  $\Delta V_{\text{thslid}}$  can be modified based on the ambient temperature measurement and charging current.

Fig. 5 presents typical experimental results that show improved performance of the proposed charging algorithm. As the figure shows, charge termination was properly determined, despite the fact that there were changing illumination conditions causing different charging currents. It is important to note that conventional, known voltage detection charge algorithms fail to properly charge the battery because they falsely terminate the charge at around  $t = 65$  min in this case. The experiment is based on charging a 12-V NiMH battery using a 30-W commercial solar panel.

This algorithm, however, is not perfect: If the algorithm resets repeatedly, it is theoretically possible that it may miss the voltage inflection point due to overcharge and therefore keep charging the battery beyond full SOC and, the algorithm may stop charging late. Also, thresholds must be carefully chosen. However, all the experiments performed showed correct behavior of the algorithm.

### B. New Differential Temperature Algorithm

To improve the robustness of the charge-control algorithm in changing environments, we propose a new charge-control algorithm that utilizes differential measurement of temperature between battery cells.

This involves separating the batteries into two (or more) groups, which we call “legs,” as they are charging inside the cradle or battery pack.

The method, illustrated in principle in Fig. 7, relies on the fact that changes in ambient conditions affect both legs the same [Fig. 7(b)]. Thus, the difference in temperature between the two legs stays close to zero unless one leg reaches full SOC [Fig. 7(c)]. When that happens, both temperature difference and the derivative of temperature difference between the two legs rise sharply. This way, full SOC can be detected in one leg by calculating the derivative of temperature difference between the legs. Of course, this assumes that the two legs are not reaching full SOC or overcharging precisely at the same time. This can be ensured if one leg is open-circuited while the other leg is charging. Our algorithm uses a pattern of charging compatible with these assumptions.

The algorithm utilizes the temperature of the two legs to perform differential temperature measurements rather than using the ambient temperature. This is because the temperature measured by the ambient temperature thermistor has different thermal time constant than the battery. Thus, it is easier to implement the algorithm by measuring two cell battery temperatures. (However, the principle could be extended to use ambient temperature also). This is illustrated and further explained in Fig. 6.

Charge balance should be maintained between the two charging battery legs [16]. Large unbalance results in reduced operational time and may even damage the battery (because of the over-charging and discharging [17] of some batteries that might result when the batteries are used in series). This would be noticeably prevalent if the user removes the batteries from the charger before each cell reaches full SOC, which is something that can be expected.

Explanation of New Temperature Differential Algorithm: The new differential temperature algorithm is shown in Fig. 8.

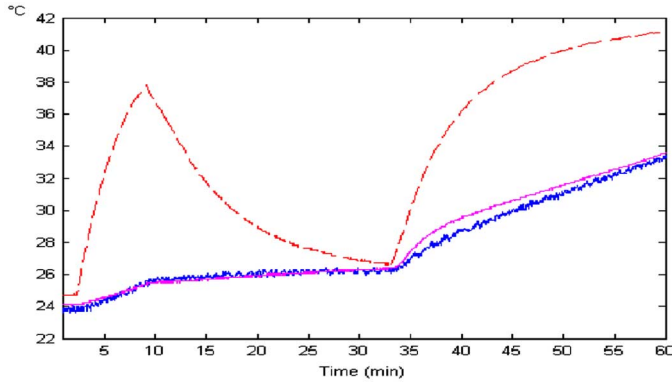


Fig. 6. Thermistor measuring ambient temperature (dashed line) that is placed in the charger free space reacts quickly to irradiation by a source of heat while the temperature inside the battery pack (solid lines, one for each leg) takes more time to react. So, differential measurement with the external thermistor loses its direct simplicity.

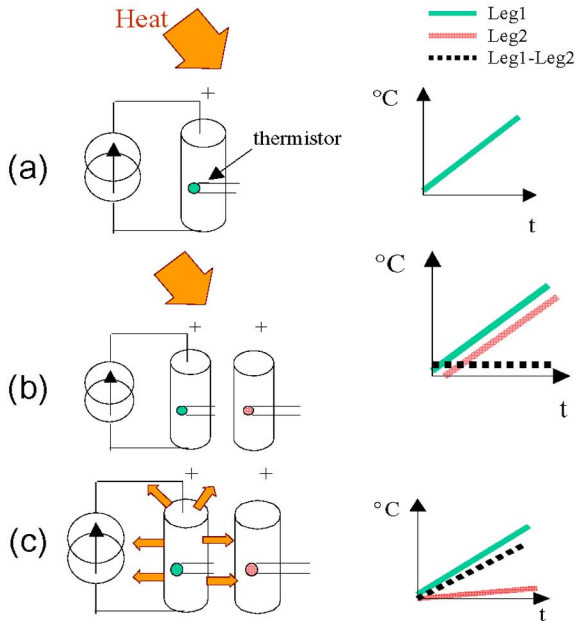


Fig. 7. (a) If there is only one leg, conventional algorithms have no way of telling whether the rise in temperature is due to the external source of heat or overcharge. (b) A second leg that is certified not overcharging (here it is open circuited) can restore the information by comparison. In this illustration, the rise is due to external heating and  $T_1 - T_2$  is relatively constant. Leg1 has not reached full SOC yet. (c) Overcharging in Leg1 creates an unbalance in the temperature and  $(T_1 - T_2)$  is rising.

The cells are separated into two groups and simultaneously charged either in parallel or through an independent charging circuit. When a high positive temperature derivative ( $thsld1$ ) is detected in one of the groups (Leg 1, for example), the algorithm switches to “potential overcharge mode”: the leg (Leg1) is kept charging while charging in the other leg (Leg2) is stopped.

The algorithm will run in this mode for a certain set time (set by timer1). During this time, if a large difference in the cells’ temperature arises [ $d(T_1 - T_2)/dt > thsld2$  and/or high  $(T_1 - T_2)$ ], then the algorithm will detect overcharge (of Leg 1 in our example). If no overcharge has been detected after a certain time, the algorithm will switch back to charging both legs. The

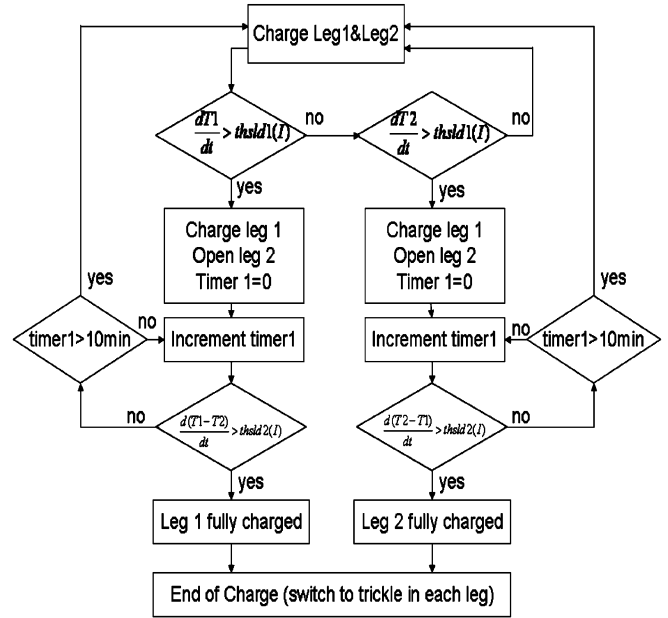


Fig. 8. Proposed charge-control algorithm. Each leg is first monitored. When high rise in temperature is detected in one leg, the charge is stopped momentarily in the other leg which becomes a “reference” leg. If a strong and fast rising differential appears ( $d(T_1 - T_2)/dt > thsld2$ ), overcharge is detected in one leg. Often, balance can be assumed. So the second leg can be assumed to be fully charged as well.

unbalance that has occurred during this time can be absorbed by either current monitoring, where the proportion of current flowing in one leg vs. the other leg is controlled, or naturally, by having the legs in parallel. Thresholds are dependant on the average charging current calculated over a sliding window of a few minutes and are stored in a lookup table. Fig. 7 gives further explanation as to why the algorithm is robust to ambient temperature changes.

C. Experimental Results for Temperature Algorithm

The charge-control experiments were performed using a sealed  $2 \times 12$  V (two 12-V legs) BB390 NiMH battery consisting of 2 sections of 20 cells (ten in series, two in parallel) and built-in thermistors for each leg. A charger implementing the algorithm of Fig. 8 was built around a PIC18F452 micro-controller. The algorithm is programmed in a micro-controller and senses the cells’ temperature through two thermistors. Some results are shown in Fig. 9. This experiment has been carried out in the lab using a lab power supply. We have chosen to put the legs in parallel when both are charging. During the charge process, the battery is heated by a strong halogen lamp (for 20 min) to simulate harsh external conditions.

- Referring to the experimental result in Fig. 9:
- the battery charging process starts at  $t = 10$  min;
  - at  $t = 20$  min, a strong heat source (a halogen lamp) is aimed at the battery. Fig. 9(d) shows the derivative of temperature of Leg1 (only Leg1 shown for more clarity);
  - at  $t = 22$  min, this value reaches a threshold, the algorithm stops the charge in Leg1, but keeps it in Leg2 (all the current is redirected to Leg2). As can be seen in Fig. 9(e), the derivative of the difference in temperatures between the

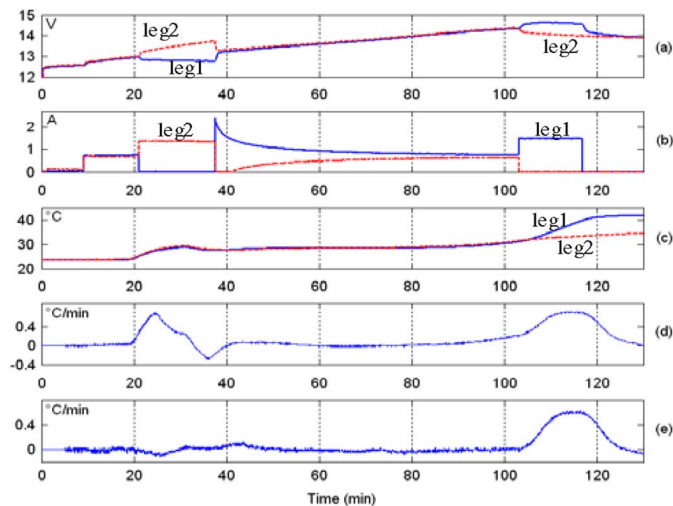


Fig. 9. (a) Voltage of the two legs. (b) Charging current in each leg. (c) Temperature of each leg. (d) Derivative of temperature at Leg1 (calculated over a sliding window of 5 min). (e) Derivative of the difference of the temperatures.

two legs stays at very low levels during that time ( $t = 22$  to  $37$  min);

- at  $t = 34$  min, the source was turned off explaining the drop in the temperature of both legs.
- at  $t = 37$  min, 15 min after, the algorithm deduces that the elevation of temperature was caused by external conditions and resumes charging both legs. During that time no charge was lost since current kept flowing in the battery at the same rate. A rebalance process is then occurring where the Leg1 (which was cut off) gets all the current from the source in addition to some current from Leg2;
- at  $t = 105$  min, a high rise in temperature is detected again, this time, stopping the charge in Leg2. This rise is due to full SOC being reached on both legs. With one leg cut off and another leg charging near full SOC, a strong differential arises in the temperatures is seen in Fig. 9(c). This results in a large derivative of the temperature difference;
- the algorithm detected full SOC at  $t = 118$  min. Note how detection based on simple  $dT/dt$  measurement would have failed in this case. As Fig. 9(d) shows, the rate of elevation at  $t = 25$  min (external heating) is comparable to that of  $t = 118$  min (one leg overcharging).

As explained above, the algorithm enters the “potential overcharge mode” on Leg2 but does not identify any overcharge and resumes charging. At that time, it can be seen that the legs naturally rebalance themselves. Leg1 receives all the current and progressively shares it again with Leg2. Both legs reach full SOC at the same time. At that moment, high temperature increase puts the algorithm again in “potential overcharge mode,” stopping momentarily the charge in Leg2. This time, overcharge will be detected on Leg1 since  $d(T_1 - T_2)/dt$  continues to sharply rise.

More curves (Figs. 10 and 11) illustrate the robustness of the charge-control algorithm when charging outdoor with a 30-W solar panel as the charging source. Experiments have been performed outdoors in Boston, Massachusetts. In Fig. 10, the battery starts the charging process at room temperature and quickly

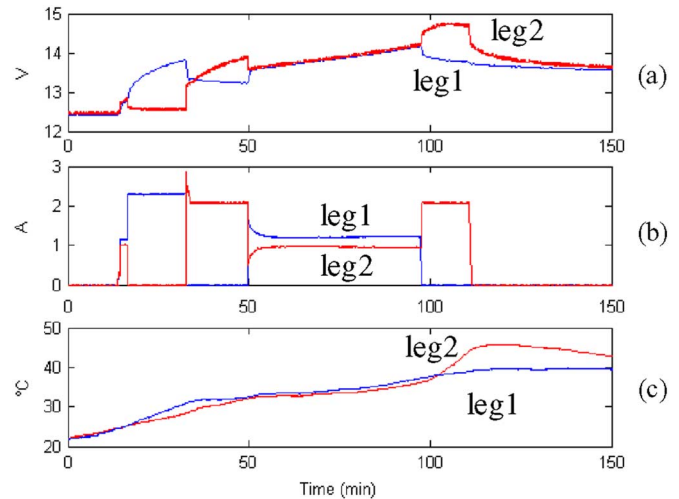


Fig. 10. (a) Voltage of the two legs. (b) Current of two legs. (c) Temperature of each leg.

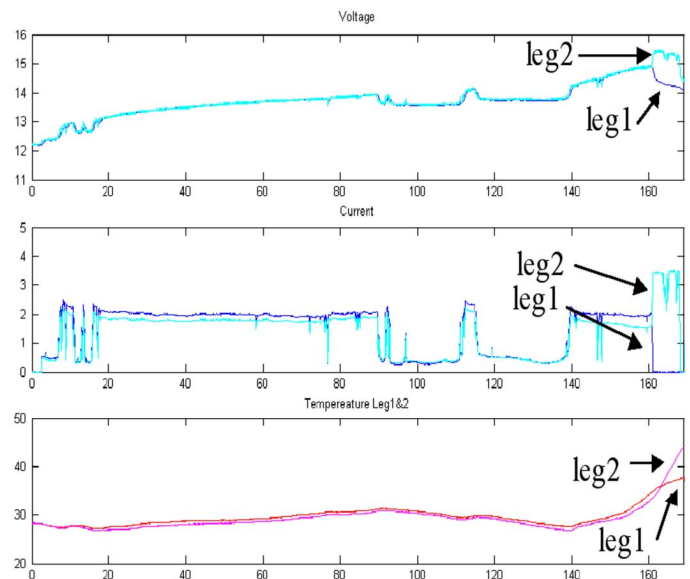


Fig. 11. Typical cloudy day outdoor experiment realized using a 30-W solar panel [1] charging the battery pack. Despite changes in the charging current as overcharge is correctly detected at  $t = 166$  min.

warms up when placed outside. This triggers a potential overcharge detection that the algorithm was able to handle. The end of charge is later accurately detected at  $t = 115$  min.

Different options exist when full SOC has been detected in one leg.

- The legs can be assumed to be balanced. In this case, the other leg can be considered to be also fully charged. The system switches to trickle charge in both legs.
- If the legs cannot be assumed to be balanced after finishing charging one leg, the algorithm has to finish charging the other leg before displaying full charge. In that case, the threshold values for overcharge detection are modified because of the high differential already created by the other leg (the one that has been detected as fully charged).
- Alternatively, if the legs were balanced at the beginning of the process, The balancing of the legs at the end of the

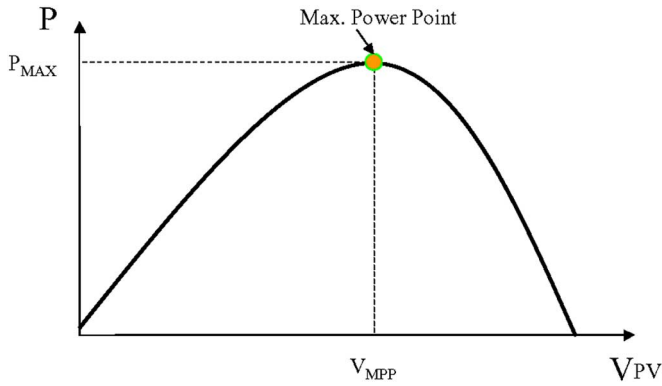


Fig. 12. Power versus voltage curve of a solar panel for a given light intensity and temperature. The voltage at which the solar panel delivers the most power is called the MPP of the solar panel.

charging process could be done using Coulomb counters to ensure that both legs receive the same amount of charge.

In the experiment shown in Fig. 9, when one leg has been detected as fully charged, the other one is assumed to be fully charged or very close to full charge as well (due to the fact that charge balance takes place throughout the charging process while the batteries are in parallel [16]), and the fast charging process ends.

Of course, the algorithm can still be fooled in condition where the heat is concentrated on only one of the legs, for example when half of the battery is shaded and the other half exposed. This would result in a strong rise in temperature as well as a strong differential rise and overcharge would falsely be detected. It should be noted, however, that such a phenomenon would also trigger false detection in the conventional algorithms. This can be shown mathematically: Suppose that one leg is totally shaded while the other leg is illuminated and not heat is exchanged between the two legs (worst case), the temperature in the first leg will stay constant (because the batteries are not fully charged at this time) while the temperature in the other leg will ramp up (because of external heating)

$$\frac{d(T_2 - T_1)}{dt} = \frac{dT_2}{dt}.$$

When used with sealed battery packs, the algorithm thresholds have to be tailored to that specific battery pack due to specific thermistors and thermal constants. When used with single cells (such as AA batteries), the thresholds depend mainly on the cradle specifications. The authors have tested several different manufacturer's NiMH cells: In our experiments, same thresholds could be used in the proposed charge algorithms for these different cells.

#### IV. MAXIMUM POWER POINT TRACKING (MPPT)

MPPT is based on the Power (P) versus Voltage (V) characteristic of a solar panel, as shown in Fig. 12. The point on the curve where the power is maximized is called the Maximum Power Point of the solar panel. By inserting a dc–dc converter between the solar panel and the load, the voltage of the solar panel can be controlled to operate at  $V_{MPP}$  and thus deliver maximum power to the load. Another advantage of this technique is that, if an up/down converter is used for the maximum

power point tracker; power can then be delivered to loads with higher voltage than the solar panel, enabling new applications for the same solar panel. MPPT is realized using a Perturb and Observe (P&O) algorithm [10], [11], [18], [19] which is a well known and efficient way to track the maximum power point of the solar panel [20], [21]. Another method is to sample the open circuit voltage and operate the PV array at a fixed fraction of that voltage [22]–[24]. However, the MPP of the panel changes with light intensity and temperature [25]. Open circuit voltage can be resampled at given times to accommodate the changes, but this method reacts slowly to change in the light intensity and the fraction of the open circuit voltage at which the solar panel operates at MPP varies with the technology of the solar panel used. Similarly, short circuit current measurement of the solar panel also provides information on the location of the MPP [23]. Incremental conductance algorithms are another method of tracking the MPP. [26]. Finally, there exist some other analog methods of finding the maximum power point relying on the dc–dc (or dc–ac) converter characteristics and operation [27]–[29]. Although this paper uses P&O for MPPT, the proposed charge-control algorithms are valid for these other MPPT methods also.

Classical P&O algorithms measure the output current and voltage of the solar panel to calculate the output power. The variable controlled is the voltage of the solar panel (input voltage of the dc–dc converter) through the duty cycle of the dc–dc converter. The dc–dc converter is therefore controlled to keep its input voltage (the voltage of the solar panel) to a desired voltage  $V_{PV}$ .

The controller first perturbs the set point of the converter by applying a  $\Delta V_{PV}$  modification (negative or positive) to the previous converter voltage set point. If the calculated power after the perturbation has increased, the controller will again change the set point by  $\Delta V_{PV}$ . If the power is decreased, the controller will change the set point by  $-\Delta V_{PV}$ . Eventually, the voltage will oscillate around the MPP of the solar panel [10], [11].

In our design, the power delivered to the battery is proportional to the amount of charging current. The voltage at the battery terminal is assumed to be  $V_{BATT} = V_0 + R_{int} \cdot I_{BATT}$  where  $V_0$  is the battery open circuit voltage,  $R_{int}$  is the internal resistance of the battery and  $I_{BATT}$  is the charging current. So

$$P_{BATT} = V_{BATT} \cdot I_{BATT} = V_0 \cdot I_{BATT} + R_{int} \cdot I_{BATT}^2.$$

Therefore, by making sure that maximum current is delivered to the battery, we make sure that maximum power is delivered as well [30]. This is only true when the battery is not connected to any load.

Also, care needs to be taken when using this simplification: since the value tracked is the power at the output of the dc–dc converter rather than the power at the output of the PV array (the way it is usually done). Local maxima could arise due to the varying efficiency of the converter at different points, since the maximum efficiency point of the dc–dc converter is not the same as the maximum power point of the solar panel. However, we did not experience any local maxima due to the dc–dc converter (SEPIC topology) in our system.

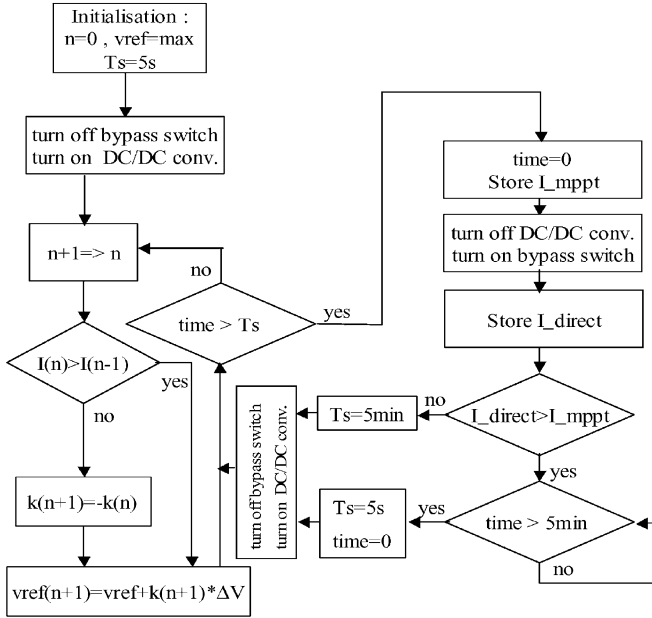


Fig. 13. Algorithm used for implementing MPPT with a bypass switch.

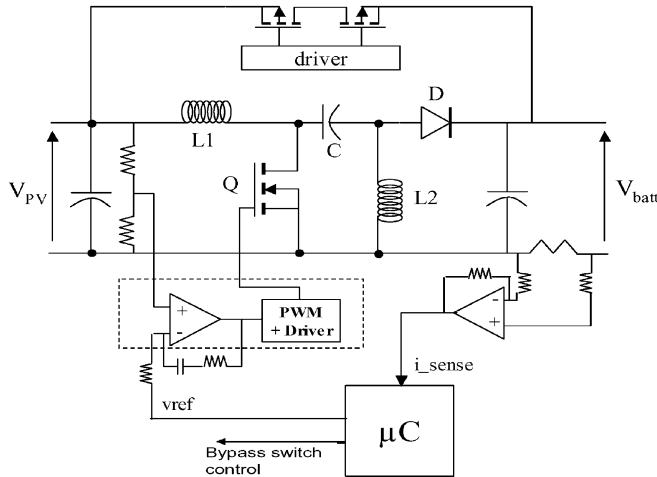


Fig. 14. Implementation of the MPPT using a Sepic converter and bypass switch. The Sepic topology was used because it offers common ground between the input and output and continuous current at the input. The bypass switch is controlled by the microcontroller.

Explanation of MPPT/Bypass Switch: Referring to Fig. 13, MPP is achieved by adjusting  $v_{ref}$  of the dc–dc converter control loop by  $k(n+1) * \Delta V$ , where  $k(\cdot) = \pm 1$ . That is,  $k = 1$ , the  $v_{ref}$  increases, and when  $k = -1$ ,  $v_{ref}$  decreases.

When the algorithm has stabilized around the Maximum Power Point (which is assumed to be done after a 5-s search), the micro-controller assesses whether MPPT increases delivered power or not. This is done by switching to direct connection and comparing the charging current delivered to the battery. The best solution will be retained. Every 5 min, the two possibilities (direct connection or MPPT) will be tried again. (in case the MPP of the solar panel changed due to light intensity or temperature).

The schematic of the circuit is shown in Fig. 14.  $L1 = L2 = 66 \mu\text{H}$ ,  $C = 88 \mu\text{F}$ ,  $Q$  is an IRF450 switching at 100 kHz and

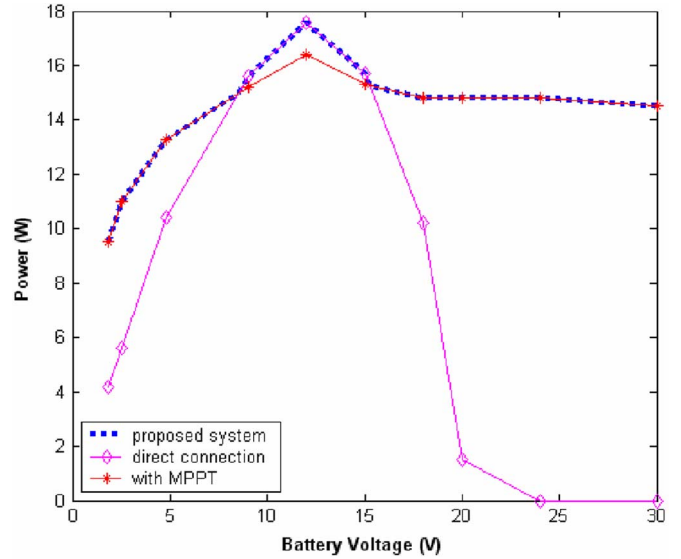


Fig. 15. Power delivered to the load as a function of the load voltage for the MPPT using the converter (red) and direct connection or bypass switch (blue). MPPT shows improvement in the charging power for various voltages.

$D$  is a Schottky diode (30CTQ045). The bypass switch consists of two series connected MOSFETs (IRF4905) to avoid reverse current from flowing to the entry of the system, especially when the converter is working. MPPT is performed by the dc–dc converter with the bypass switch off. Improvement in the charging rate is presented in Fig. 15 for a variety of batteries. Fig. 15 shows the power delivered to the load as a function of the load voltage for a given light intensity. Solar panels are often manufactured to optimally charge a specific terminal battery voltage. For example, the 30 W panels used in our experiments are made to charge 12-V batteries and have a  $V_{MPP}$  around 14 V. Thus, there is a range of load voltage for which MPPT actually reduces the power delivered to the battery. This is due to the power dissipation in the converter. To avoid this loss, the bypass switch can be used to create an optional direct connection between the solar panel and the battery. This reduces the losses through the system when the load voltage is matching the solar panel voltage and the bypass switch is activated.

Notice in Fig. 15 that MPPT increases charging current for a broad range of battery voltage, for  $V_{batt} > 15 \text{ V}$  and  $V_{batt} < 12 \text{ V}$ . The PV module is built to have optimized output power around 12 V. Therefore, for a 12-V battery the micro-controller selects to charge through the bypass switch instead of the dc–dc converter, thus eliminating the losses in the dc–dc converter. In this case, the solar array is directly connected to the battery. Thus, the power delivered to the battery with the new charge controller is given by the dashed curve in Fig. 15; i.e.,  $P_{charger} = \max\{P_{direct\ connection}, P_{DC/DC}\}$ . Also, without the MPPT, it would not be feasible to charge batteries above 24 V, since the PV cannot produce a current at such a high voltage.

## V. CONCLUSION

In this paper, we have shown that existing NiMH charge-control algorithms fail in changing environmental conditions

(changing weather, changing current). This paper proposes new charge-control algorithms to overcome this problem. The new algorithms are more robust to variations in current and temperature (although false detection cannot be completely ruled out). Because more data is required to perform the analysis, this technique is likely to be more expensive. It should be noted, however, that the overall charger size is still small ( $2 \times 3$  inches, without MPPT) despite the fact that no specialized IC is used. The increase in complexity of the charger is a direct consequence of the charging process taking place in a much more perturbed environment. The increase in the cost resulting from the use of a microcontroller vs. a dedicated IC can be compensated to some extent by the addition of extra features such as MPPT control at no extra cost. By adding a Maximum Power Point Tracker within the controller, higher charging current can often be achieved. This quickens charging time and adds flexibility to the overall system because it becomes able to efficiently charge batteries with wide terminal voltage. Although the proposed chargers are designed for NiMH batteries, they can be directly used for NiCd batteries by adjusting thresholds.

#### REFERENCES

- [1] Portable Solar Array Datasheet From Global Solar pp. 3–48 [Online]. Available: [http://www.globalsolar.com/sheet/p3\\_48Specs.pdf](http://www.globalsolar.com/sheet/p3_48Specs.pdf)
- [2] A. Gregg, R. Blieden, A. Chang, and H. Ng, "Performance analysis of large scale, amorphous silicon, photovoltaic power systems," *Rec. IEEE Photovoltaic Specialists Conf.*, pp. 1615–1618, Jan. 2005.
- [3] P. Fairley, "Solar-Cell Rollout," *Technol. Rev.*, vol. 107, no. 6, pp. 34–40, July 2004.
- [4] E. Koutroulis and K. Kalaitzakis, "Novel battery charging regulation system for photovoltaic applications," *Proc. Inst. Elect. Eng.*, vol. 151, no. 2, pp. 191–197, Mar. 2004.
- [5] G. Danese, F. Leporati, R. Lombardi, M. Nucita, G. Pedrazzini, and G. Ricotti, "An instrument for the characterization of voltage and temperature profile in NiCd and NiMH batteries," in *Proc. 23rd Euromicro Conf.*, Budapest, Hungary, Sep. 1997, pp. 178–183.
- [6] M. Gonzalez, M. A. Perez, J. C. Campo, and F. J. Ferrero, "Accurate detection algorithm of battery full-capacity under fast-charge," in *Proc. Instrumentation and Measurement Technology Conf.*, May 1998, pp. 755–759.
- [7] C. B. Falcon, "Temperature termination and the thermal characteristics of NiCd and NiMH batteries," in *WESCON/94. 'Idea/Microelectronics' Conf. Rec.*, Sep. 1994, pp. 309–315.
- [8] M. Gonzalez, F. J. Ferrero, J. C. Anton, and M. A. Perez, "Considerations to improve the practical design of universal and full-effective NiCd/NiMH battery fast-chargers," in *Applied Power Electronics Conf. and Expo.*, 1999, vol. 1, pp. 167–173.
- [9] F. Lima, J. N. Ramalho, D. Tavares, J. Duarte, C. Albuquerque, T. Marques, A. Gerales, A. P. Casimiro, G. Renkema, J. Been, and W. Groeneveld, "A novel universal battery charger for NiCd, NiMH, Li-ion and Li-polymer," in *Proc. Conf. Eur. Solid-State Circuits*, 2003, pp. 209–212.
- [10] E. Koutroulis, K. Kalaitzakis, and N. C. Voulgaris, "Development of a microcontroller-based, photovoltaic maximum power point tracking control system," *IEEE Trans. Power Electron.*, vol. 16, no. 1, pp. 46–54, Jan. 2001.
- [11] C. R. Sullivan and M. J. Powers, "A high-efficiency maximum power point tracker for photovoltaic arrays in a solar-powered race vehicle," in *IEEE Power Electronics Specialists Conf.*, Jun. 1993, pp. 574–580.
- [12] O. Barbarisi, R. Canaletti, L. Glielmo, M. Gosso, and F. Vasca, "State of charge estimator for NiMH batteries," in *Proc. 41st IEEE Conf. Decision and Control*, 2002, vol. 2, pp. 1739–1744.
- [13] T. D. Hund and B. Thompson, "Amp-hour counting charge control for photovoltaic hybrid power systems," in *Rec. 26th Photovoltaic Specialists Conf.*, Sep. 1997, pp. 1281–1284.
- [14] Brentronics' BB-390 B/U Datasheet [Online]. Available: [www.brentronics.com/pdf/BB390B.pdf](http://www.brentronics.com/pdf/BB390B.pdf)
- [15] K. Bundy, M. Karlsson, G. Lindbergh, and A. Lundqvist, "An electrochemical impedance spectroscopy method for prediction of the state of charge of a nickel-metal hydride battery at open circuit and during discharge," *J. Power Sources*, vol. 72, no. 2, pp. 118–125, Apr. 1998.
- [16] A. Hande and T. A. Stuart, "A selective equalizer for NiMH batteries," *J. Power Sources*, vol. 138, no. 1–2, pp. 327–339, Nov. 2004.
- [17] W. K. Hu, M. M. Geng, X. P. Gao, T. Burchardt, Z. X. Gong, D. Noréus, and N. K. Nakstad, "Effect of long-term overcharge and operated temperature on performance of rechargeable NiMH cells," *J. Power Sources*, vol. 159, no. 2, pp. 1478–1483, Sept. 2006.
- [18] N. Femia, G. Petrone, G. Spagnuolo, and M. Vitelli, "Optimization of perturb and observe maximum power point tracking method," *IEEE Trans. Power Electron.*, vol. 20, no. 4, pp. 963–973, Jul. 2005.
- [19] M. Veerachary, T. Senjyu, and K. Uezato, "Maximum power point tracking of coupled inductor interleaved boost converter supplied PV system," *Proc. Inst. Elect. Eng.*, vol. 150, no. 1, pp. 71–80, Jan. 2003.
- [20] D. P. Hohm and M. E. Ropp, "Comparative study of maximum power point tracking algorithms using an experimental, programmable, maximum power point tracking test bed," in *Proc. 28th IEEE Photovoltaic Specialists Conf.*, Sep. 2000, pp. 1699–1702.
- [21] V. Salas, M. J. Manzanar, A. Lazaro, A. Barrado, and E. Olias, "The control strategies for photovoltaic regulators applied to stand-alone systems," in *Proc. IECON'02*, Nov. 2002, vol. 4, pp. 3274–3279.
- [22] J. H. R. Enslin, M. S. Wolf, D. B. Snyman, and W. Swiegers, "Integrated photovoltaic maximum power point tracking converter," *IEEE Trans. Ind. Electron.*, vol. 44, no. 6, pp. 769–773, Dec. 1997.
- [23] M. A. S. Masoum, H. Dehbonei, and E. F. Fuchs, "Theoretical and experimental analyses of photovoltaic systems with voltage and current-based maximum power point tracking," *IEEE Trans. Energy Convers.*, vol. 17, no. 4, pp. 514–522, Dec. 2002.
- [24] M. A. S. Masoum, S. M. Mosavi, and E. F. Fuchs, "A Microprocessor controlled new class of optimal battery chargers for photovoltaic applications," *IEEE Trans. Energy Convers.*, vol. 19, no. 3, pp. 599–606, Sep. 2004.
- [25] E. Radziemska and E. Klugmann, "Photovoltaic maximum power point varying with illumination and temperature," *J. Solar Energy Eng.*, vol. 128, no. 1, pp. 34–39, Feb. 2006.
- [26] K. H. Hussein, I. Muta, T. Hoshino, and M. Osakada, "Maximum photovoltaic power tracking: An algorithm for rapidly changing atmospheric conditions," *Proc. Inst. Elect. Eng.*, vol. 142, no. 1, pp. 59–64, Jan. 1995.
- [27] H. S. Chung, K. K. Tse, S. Y. R. Hui, C. M. Mok, and M. T. Ho, "A novel maximum power point tracking technique for solar panels using a SEPIC or Cuk converter," *IEEE Trans. Power Electron.*, vol. 18, no. 3, pp. 717–724, May 2003.
- [28] A. Brambilla, M. Gambarara, A. Garutti, and F. Ronchi, "New approach to photovoltaic arrays maximum power point tracking," in *Proc. IEEE Power Electronics Specialists Conf.*, Jul. 1999, vol. 2, pp. 632–637.
- [29] P. Midya, P. T. Krein, R. J. Turnbull, R. Reppa, and J. Kimball, "Dynamic maximum power point tracker for photovoltaic applications," in *Proc. IEEE Power Electronics Specialists Conf.*, Jun. 1996, vol. 2, pp. 1710–1716.
- [30] D. Shmilovitz, "On the control of photovoltaic maximum power point tracker via output parameters," *Proc. Inst. Elect. Eng.*, vol. 152, no. 2, pp. 239–248, Mar. 2005.



**Florent Boico** was born in Rehovot, Israel, in 1979. He received the Diplôme d'Etudes Approfondies in robotics and intelligent systems from Université Pierre et Marie Curie (Paris 6), Paris, France, in 2003. He is currently pursuing the Ph.D. degree in electrical engineering at Northeastern University, Boston, MA.  
His research interests include dc-dc converters, battery charging, and photovoltaics.



**Brad Lehman** (M'95) received the B.S. degree from the Georgia Institute of Technology, Atlanta, in 1987, the M.S. degree from the University of Illinois at Champaign-Urbana, in 1988, and the Ph.D. degree from the Georgia Institute of Technology, Atlanta, in 1992, all in electrical engineering.

He is presently an Associate Professor in the Department of Electrical and Computer Engineering, Northeastern University, Boston, MA, and, beforehand, was a Hearin Hess Distinguished Assistant Professor at Mississippi State University. He was previously an NSF Presidential Faculty Fellow, a Visiting Scientist at the Massachusetts Institute of Technology (MIT), and the head swimming and diving coach at the Georgia Institute of Technology. He performs research in the areas of power electronics, with a primary focus of his research is in the modeling, design and control of dc-dc converters with applications to high brightness LEDs, battery chargers, telecommunication power supplies, and VRMs.

Dr. Lehman received the Alcoa Science Foundation Fellowship and serves as an Associate Editor of the IEEE TRANSACTIONS ON POWER ELECTRONICS. From 1993 to 1997, he served as an Associate Editor for the IEEE TRANSACTIONS ON AUTOMATIC CONTROL. In 1999, he served as a Science Advisor to the to Commonwealth of Massachusetts, Science and Technology Committee (State Senate) for the Y2K issue in the Power Industry.

**Khalil Shujaee**, photograph and biography not available at the time of publication.